

## The streamer-to-spark transition in a transient spark: a dc-driven nanosecond-pulsed discharge in atmospheric air

This article has been downloaded from IOPscience. Please scroll down to see the full text article.

2012 Plasma Sources Sci. Technol. 21 045006

(<http://iopscience.iop.org/0963-0252/21/4/045006>)

View [the table of contents for this issue](#), or go to the [journal homepage](#) for more

Download details:

IP Address: 158.195.84.207

The article was downloaded on 21/06/2012 at 08:27

Please note that [terms and conditions apply](#).

# The streamer-to-spark transition in a transient spark: a dc-driven nanosecond-pulsed discharge in atmospheric air

Mário Janda, Zdenko Machala, Adriana Niklová and Viktor Martišovič

Division of Environmental Physics, Faculty of Mathematics, Physics and Informatics, Comenius University, Mlynska dolina F2, 84248 Bratislava, Slovakia

E-mail: [janda@fmph.uniba.sk](mailto:janda@fmph.uniba.sk)

Received 14 February 2012, in final form 3 May 2012

Published 20 June 2012

Online at [stacks.iop.org/PSST/21/045006](http://stacks.iop.org/PSST/21/045006)

## Abstract

We present a study of the streamer-to-spark transition in a self-pulsing dc-driven discharge called a transient spark (TS). The TS is a streamer-to-spark transition discharge with short spark duration ( $\sim 10$ – $100$  ns), based on charging and discharging of the internal capacity of the electric circuit with repetition frequency 1–10 kHz. The TS can be maintained under relatively low energy conditions ( $0.1$ – $1$  mJ pulse $^{-1}$ ). It generates a very reactive non-equilibrium air plasma applicable for flue gas cleaning or bio-decontamination.

Thanks to the short spark current pulse duration, the steady-state gas temperature, measured at the beginning of the streamers initiating the TS, increases from an initial value of  $\sim 300$  K only up to  $\sim 550$  K at 10 kHz. The streamer-to-spark transition is governed by the subsequent increase in the gas temperature in the plasma channel up to  $\sim 1000$  K. This breakdown temperature does not change with increasing repetition frequency  $f$ . The heating after the streamer accelerates with increasing  $f$ , leading to a decrease in the average streamer-to-spark transition time from a few  $\mu$ s to less than 100 ns.

(Some figures may appear in colour only in the online journal)

## 1. Introduction

A non-thermal atmospheric-pressure plasma can induce chemical reactions in otherwise inert gas mixtures [1–3] without significantly heating them, thus keeping energy consumption relatively low. The desired chemical effect is achieved by efficient production of reactive radicals by the collisions of high-energy electrons with neutral species. In order to break chemical bonds, the mean energy of the electrons should be at least around 1 eV. The density of the electrons must be also high enough to ensure efficient conversion of reactants to products. The easiest way to meet these conditions without heating the neutral species is to use an external electric field.

Electrons can easily gain sufficient energy from the applied electric field, because they lose only a small fraction in elastic collisions with neutral species. Once they have enough energy, their density starts to grow thanks to electron-impact ionization processes, resembling the development of

an avalanche. At atmospheric pressure, an electron avalanche transforms to a streamer once the space charge exceeds a critical value, the so-called Meek's criterion [4].

A streamer is an ionization wave propagating in the region with strong field from the high-voltage (HV) electrode towards the grounded electrode. Thanks to the space charge, the electric field in the streamer's head can reach more than  $200$  kV cm $^{-1}$  [5, 6], so that the chemical and ionization processes are very efficient there. Streamers are thus considered to be crucial for the efficiency of plasma-induced chemistry at atmospheric pressure. However, a streamer may also lead to an electrical breakdown if it reaches the opposite electrode and creates a conductive plasma bridge between them.

Electrical breakdown is a crucial issue for the generation of electrical discharges, as well as in the design of HV devices. The first studies of this phenomenon appeared several decades ago [7–9] and the streamer breakdown theory was introduced

by Meek [4], Raether [10] and Loeb [11] in the middle of the 20th century. However, because of the complexity of this problem, the study of the breakdown mechanism, streamers and their propagation has continued [5, 6, 12–18].

Electrical breakdown typically leads to the formation of a spark or an arc discharge, depending on the power supply and the external electric circuit parameters. An arc or spark usually generates a thermal plasma, where the energy of all species is more or less equal and the gas is heated to very high temperatures  $T_g$ . For many applications, very high  $T_g$  and waste of energy in gas heating are not desirable. Several strategies were therefore developed to avoid the breakdown and streamer-to-spark transition. Two of the most common methods are based on covering at least one electrode with an insulator (e.g. a dielectric barrier discharge [3, 19, 20]) or using very short HV pulses [2, 21–26].

A restriction of thermal plasma generation can also be achieved when using a dc power supply by adding a ballast resistor ( $R > 1 \text{ M}\Omega$ ) to limit the discharge current. Several types of electrical discharges producing a non-thermal plasma can be generated in this way, depending on the electric circuit parameters, gas composition, flow rate and geometry of the electrodes [27–32].

Despite the used dc power supply, some of these discharges have a pulsed character, such as a prevented spark (PS), developed by the group of Marode [27, 33–35]. In a PS, the streamer-to-spark transition is not stopped, as in the pulsed discharges generated by pulsed HV power supplies, but the spark current peak is limited by an additional resistor between the discharging external capacitance and the gap. In this way it is possible to prevent the thermalization of the plasma during the spark phase, and even to enhance the chemical effect thanks to a so-called secondary streamer [35].

In this paper, we report the study of a filamentary pulsed discharge called a transient spark (TS), similar to the PS. The TS is initiated by a streamer, followed by a short ( $\sim 10$ – $100$  ns) high current ( $\sim 1$ – $10$  A) pulse. A transition to a typical arc or a spark discharge is also inhibited by components of the electric circuit: a large external resistor  $R$  ( $5$ – $10 \text{ M}\Omega$ ) and a small internal capacitance  $C$  ( $10$ – $40$  pF) are discharged, but the current peak is not limited in its amplitude, although it is limited in its duration. The process of periodical charging and discharging of  $C$  repeats with a characteristic frequency of a few kHz and it can be controlled by the applied dc voltage.

The increasing repetition frequency of the HV pulses up to 200 Hz in pulsed discharges has demonstrated an improved efficiency of removal of various pollutants [23]. HV pulsed devices working at repetition frequencies  $f$  above 1 kHz appeared only recently [24–26, 36], and the importance of the high repetition frequency on power efficiency of the plasma generation was also emphasized [25, 26, 36]. Thus, the high repetition frequency of a TS discharge can certainly play an important role in its chemical efficiency. However, we observed changes in some electrical and optical characteristics of the TS with increasing  $f$  [37, 38]: smaller current pulses and a disappearance of atomic lines, which seem to contradict this statement.

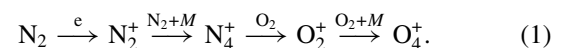
In order to understand the changes of TS characteristics with  $f$ , we performed a time-resolved optical emission

spectroscopic (OES) study, using a fast photomultiplier tube (PMT), as well as a fast iCCD camera coupled with a spectrometer. The OES technique can provide valuable information on excited atomic and molecular states. It enables one to determine the rotational, vibrational and electronic excitation temperatures of the plasma and thus the level of non-equilibrium and gas temperature [39, 40]. It was also successfully applied for the time evolution of rotational temperature  $T_r$  continuously from the primary streamer to the secondary streamer, using the second positive system of nitrogen [41].

Our results presented in this paper are also interesting for the understanding of the streamer-to-spark transition process, which is not yet fully explained. The TS enables one to study two interesting features: the influence of a large external resistor and the influence of the increasing repetition frequency on the breakdown. The influence of a large external resistor on the breakdown was already experimentally studied by Larsson [14]. The major influence of  $R$  was found to be the extension of streamer-to-spark transition delay time. This was later theoretically supported by Naidis [15]. However, Larsson used a pulsed voltage generator with low repetition frequency, so that breakdowns did not influence each other, i.e. each breakdown occurred in a ‘virgin’ gas. Moreover, his applied voltage typically highly exceeded the threshold breakdown voltage. In a TS, the breakdown occurs when the applied voltage reaches the threshold breakdown value.

### 1.1. Theory of the streamer-to-spark transition

As already mentioned, the ionization processes are very efficient in the streamer’s head. However, the electric field behind this head is weak and the plasma produced is in the decay phase. The electron density is initially decreased by a factor of ten through the dissociative recombination of electrons with  $\text{O}_4^+$  ions [16]. Afterwards, about 100 ns later, the three-body attachment on  $\text{O}_2$  becomes the most important electron sink mechanism. The  $\text{O}_4^+$  ions are built up according to the following scheme:



This conversion is fast (within a few nanoseconds) and it is necessary for the decrease in electron density, because the rate coefficient of electron recombination with  $\text{O}_4^+$  is about two orders of magnitude higher than rate coefficients of reactions with  $\text{O}_2^+$  and  $\text{N}_2^+$  ions [42, 43].

There must be another process that balances the electron loss processes and finally enables the breakdown by accelerating the ionization processes. According to Marode [35], there are three possible mechanisms.

- *Attachment control processes.* The distribution of the attachment rate along the plasma filament produced by the streamer produces an increase in the reduced electric field  $E/N$  near the anode [44–46]. At least 80 Td prevails here and the plasma-induced chemistry may be efficiently activated [47]. This region was also called a secondary streamer by Loeb, who supposed that it is a new ionization

wave [11]. A decrease in gas density leads to the extension of this region which finally reaches the cathode, as was shown in a model of Bastien and Marode [45]. Then the spark may start because  $E/N$  becomes high enough along the whole plasma filament.

- *Chemical and stepwise ionization.* The accumulation of excited metastable species can lower the threshold electron-impact ionization energy (stepwise ionization) [15]. Lowke [13] stressed the role of molecular oxygen metastable species  $O_2(a^1\Delta_g)$ . Their collisions with  $O_2^-$  ions can induce electron detachment even at room temperature.
- *Gas density decrease.* This mechanism is based on the gas heating in the plasma channel [48]. The increase in the gas temperature  $T_g$  in the channel leads to an increase in the pressure. This is followed by a hydrodynamic channel expansion that empties the core of the channel and decreases the gas density  $N$ . For this reason, a reduced electric field strength  $E/N$  in the plasma channel increases and accelerates the electron-impact ionization reactions.

The increase in  $T_g$ , mentioned in the third mechanism, may also have a direct effect on the gas phase chemistry [46]. The rate coefficients usually strongly depend on  $T_g$ . Elementary processes causing the loss of electrons include electron-ion recombination reactions and electron attachment reactions producing negative molecular ions with much lower mobility. The regeneration of electrons from these ions by thermal detachment is actually considered by many authors to be the most important mechanism responsible for maintaining the conductivity of the streamer for a period of 1–10  $\mu$ s [49–52]. To overcome the electron affinity, the gas in the channel must be heated above a critical value of 1000–2000 K so that the rate of these thermal detachment reactions is large enough. Moreover, the rate coefficients of electron-ion recombination reactions also decrease with increasing gas temperature [42, 43].

## 2. Experimental setup

A dc HV power supply connected to a stainless steel needle HV electrode via a series resistor ( $R = 4.92\text{--}9.84\text{ M}\Omega$ ) was used to generate a positive TS discharge. The distance  $d$  between the tip of the HV electrode and a grounded planar steel electrode was 4–6 mm. The experiments were carried out at room temperature in atmospheric-pressure air with a weak flow of about  $20\text{ cm s}^{-1}$ , perpendicular to the HV needle electrode.

An additional small resistor  $r = 1\text{ k}\Omega$  was attached directly to the HV electrode, thus separating it from the HV cable connecting it with the resistor  $R$ . The role of  $r$  was to eliminate the oscillations of electric signals caused by internal inductances of the HV cable and of a grounding wire. The discharge voltage was measured by an HV probe Tektronix P6015A and the discharge current was measured on a  $50\ \Omega$  or  $1\ \Omega$  resistor shunt. The  $1\ \Omega$  resistor shunt was used when we focused on TS current pulse itself, whereas the  $50\ \Omega$  resistor shunt was used to measure current from the streamer. Both voltage and current signals were recorded by a 200 MHz digitizing oscilloscope Tektronix TDS2024.

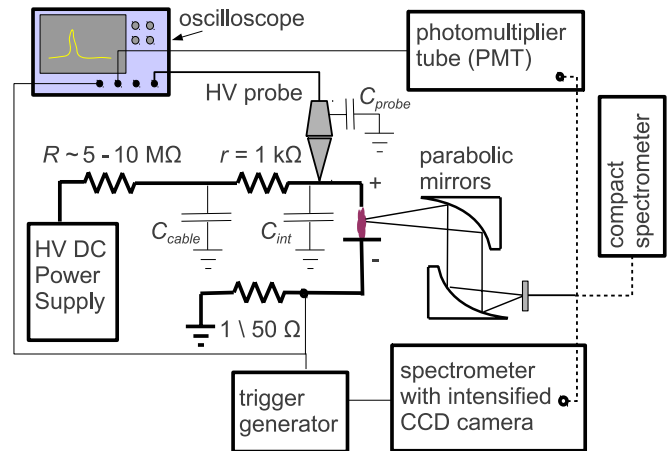


**Figure 1.** Schematic of the experimental set-up: HV, high voltage;  $R, r$ , resistors;  $C_{\text{cable}}, C_{\text{probe}}, C_{\text{int}}$ , capacitances.

For fast recording of time-integrated spectra of a broad spectral region we used a two-channel compact emission spectrometer Ocean Optics SD2000 (200–1100 nm, resolution 0.6–1.7 nm). The time-resolved emission spectra were obtained using a 2 m monochromator Carl Zeiss Jena PGS2 (resolving power 45000), covering the UV and VIS regions (200–800 nm), coupled with an intensified CCD camera (Andor Istar) with a 2 ns minimum gate. The iCCD camera was triggered by a generator of 5 V rectangular pulses with a rise time of less than 5 ns. This generator was triggered directly by the current signal, causing an additional delay of less than 10 ns. This delay, plus the delay caused by the transmission of the signal by BNC cables, was compensated for using a 10 m long optical cable (Ocean Optics P400-10-UV-VIS).

For fast measurements of the evolution of the emission intensity, we used a PMT module with a 2.2 ns rise time (Hamamatsu H955). Its signal was recorded using the oscilloscope. Whenever it was necessary to isolate a specific spectral transition for PMT measurements, a band-pass interference filter, e.g. Melles Griot 03 FIU127 for the  $N_2(C-B, 0-0)$  transition, was inserted into the optical path. The collection of light was provided by a pair of parabolic mirrors focused on a small area near the tip of the HV electrode. These mirrors, together with the optical fiber core diameter, determined the spatial resolution to be  $300\ \mu\text{m}$ . The experimental set-up is depicted in figure 1.

## 3. Results and discussion

### 3.1. Introduction to the TS

When a high voltage applied to the needle electrode is progressively increased, we first observe a streamer corona. As the voltage on the needle electrode  $U$  achieves a breakdown value  $U_{\text{TS}}$ , a transition to a TS may occur. This happens when a streamer crosses the whole gap and creates a relatively conductive plasma bridge, through which the capacitance  $C$  of the circuit can be discharged. This capacitance is composed of several components: the internal capacitance of the discharge chamber  $C_{\text{int}}$ , the capacitance of the HV probe  $C_{\text{probe}}$  and

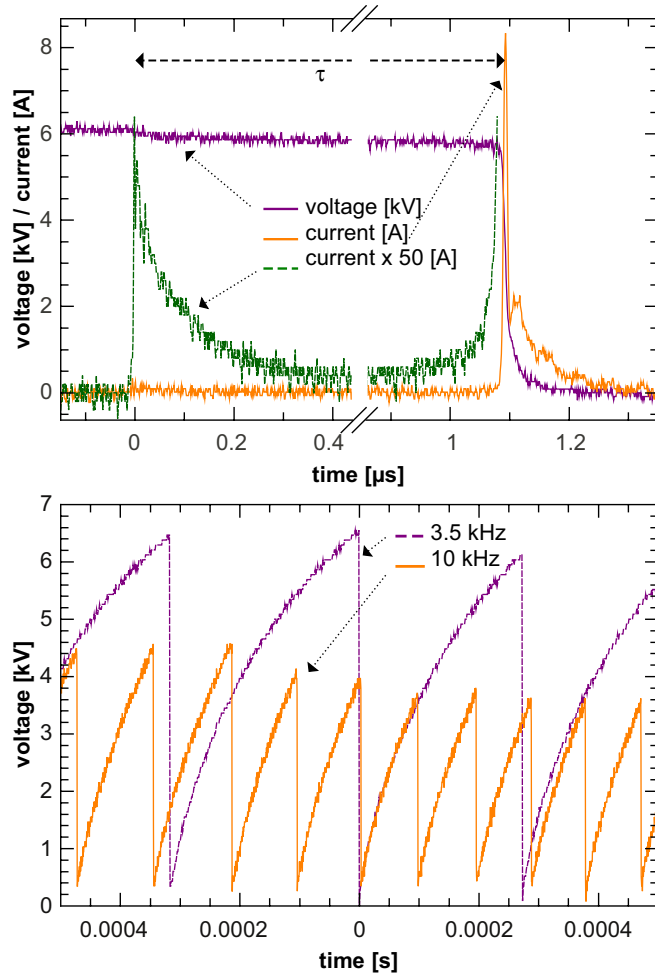


**Figure 2.** Typical waveforms of the TS in (a)  $\mu\text{s}$  time scale ( $f \approx 3 \text{ kHz}$ ), (b) ms time scale,  $R = 6.6 \text{ M}\Omega$ ,  $C = 32 \pm 4 \text{ pF}$ ,  $d = 5 \text{ mm}$ ,  $r = 1 \text{ k}\Omega$ ,  $\tau$  is the streamer-to-spark transition time.

the capacitance of the HV cable  $C_{\text{cable}}$  connecting the needle electrode with the ballast resistor  $R$  (figure 1).

When  $C$  is discharged, the current, approximately given by

$$I(t) \approx -C \times \frac{dU(t)}{dt}, \quad (2)$$

reaches a high value ( $\sim 1 \text{ A}$ ) and the voltage  $U$  drops to zero (figure 2(a)). Then, during the quenched phase,  $U$  grows in time  $t$  (figure 2(b)) according to the following equation:

$$U(t) = U_{\infty} \left[ 1 - \exp\left(\frac{-t}{RC}\right) \right], \quad (3)$$

where  $U_{\infty}$  is the generator voltage, and  $C$  is recharged.

As soon as  $U$  reaches the characteristic TS breakdown voltage  $U_{\text{TS}}$ , a new TS pulse appears. It occurs in time  $t = T$ , from which we obtain the characteristic repetition frequency  $f$  of this process:

$$f = \frac{1}{T} = \frac{1}{RC \ln \left[ \frac{U_{\infty}}{U_{\infty} - U_{\text{TS}}} \right]}. \quad (4)$$

For typical  $R$  and  $C$ , the repetition frequency  $f$  is of the order of several kHz, and it can be controlled by the generator voltage

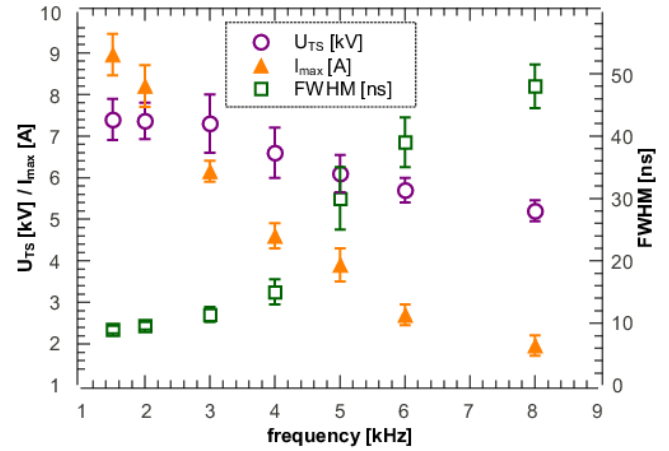


**Figure 3.** The dependence of peak current ( $I_{\text{max}}$ ), breakdown voltage  $U_{\text{TS}}$  and FWHM of the current pulses on frequency;  $C = 32 \pm 4 \text{ pF}$ ,  $r = 1 \text{ k}\Omega$ ,  $d = 5.5 \text{ mm}$ .

$U_{\infty}$ . The control of the TS by other external circuit parameters was described in detail recently [38]. A more accurate version of equation (2), which takes into account the influence of  $r$ , was also provided therein.

### 3.2. Changes in the TS electrical characteristics with $f$

The increase in the generator voltage  $U_{\infty}$  leads to a monotonic increase in  $f$ , as can also be derived from equation (4). However, the repetition frequency is not absolutely regular. It strongly depends also on  $U_{\text{TS}}$ , and each TS pulse may appear at a slightly different value of  $U_{\text{TS}}$  (figure 2(b)). We can therefore only define an average frequency, determined by an average value of  $U_{\text{TS}}$ .

Even if we know the precise value of  $U_{\text{TS}}$ , obtained at low TS repetition frequency, a further increase in  $f$  cannot be easily calculated from the external electrical parameters ( $U_{\infty}$ ,  $C$ ,  $R$ ) according to (4). We found that  $U_{\text{TS}}$  itself is a function of  $f$ ; it tends to decrease as  $f$  increases (figure 3). The increase in  $f$  is associated with changes in other TS properties as well. Current pulses get smaller and broader with increasing  $f$  (figures 3 and 4).

### 3.3. Streamer-to-spark transition time

An average streamer-to-spark transition time  $\tau$  shortens significantly with increasing  $f$  (figure 5). This is analogous with the shortening of  $\tau$  with increasing mean discharge current in the PS [33]. We also observed the prolongation of  $\tau$  with increasing  $R$  as reported by Larsson [14] and Naidis [15]. However, with a further increase in  $f$ , the influence of  $R$  becomes negligible and the average streamer-to-spark transition time shortens down to  $\sim 100 \text{ ns}$ .

The shortening of  $\tau$  and changes in the streamer versus spark peak current ratio are also partly responsible for the modification of the shape of the spark current pulse raising edge (figure 4). At lower frequencies ( $< 3 \text{ kHz}$ ),  $\tau$  is very random and it can vary from a few hundred ns up to several  $\mu\text{s}$ . The streamer and spark current pulses are well separated,

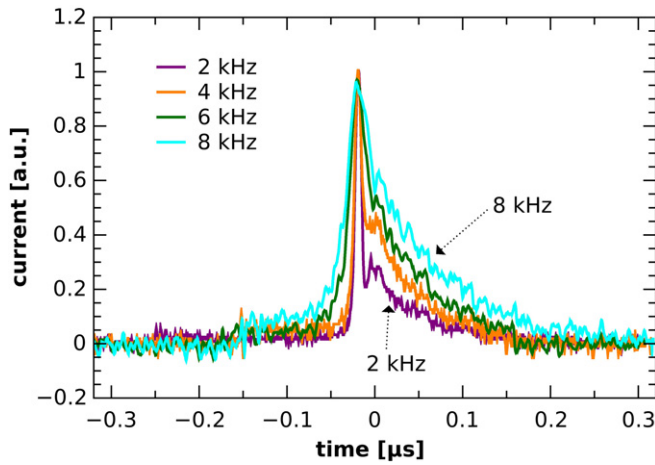


**Figure 4.** Changes of the normalized current waveforms measured on  $1 \Omega$  with increasing frequency;  $C = 32 \pm 4 \text{ pF}$ ,  $r = 1 \text{ k}\Omega$ ,  $d = 5.5 \text{ mm}$ ,  $R = 6.6 \text{ M}\Omega$ .

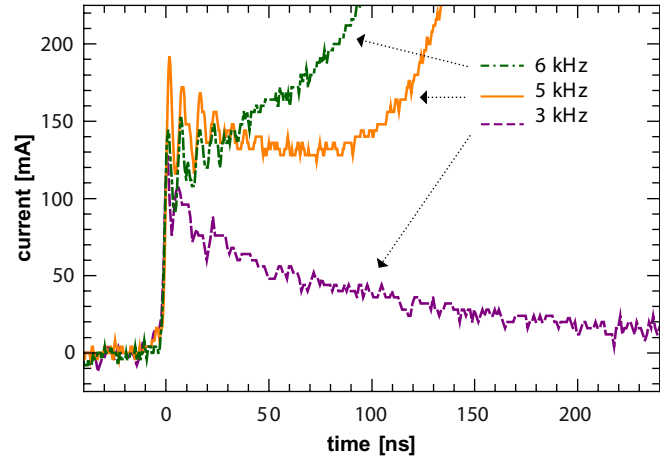


**Figure 6.** Changes in the streamer current pulses measured on  $50 \Omega$  with increasing frequency;  $C = 32 \pm 4 \text{ pF}$ ,  $r = 1 \text{ k}\Omega$ ,  $d = 5.5 \text{ mm}$ ,  $R = 8.2 \text{ M}\Omega$ .

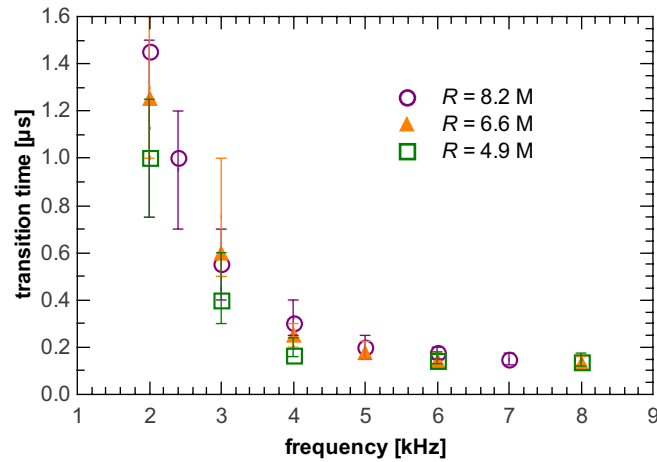


**Figure 5.** The dependence of averaged streamer-to-spark transition time on frequency;  $C = 32 \pm 4 \text{ pF}$ ,  $r = 1 \text{ k}\Omega$ ,  $d = 5.5 \text{ mm}$ .

and the streamer peak current ( $\sim 100 \text{ mA}$ ) is much smaller compared with the spark pulse ( $\sim 10 \text{ A}$ ). Moreover, since  $\tau$  is long enough, the current after the streamer pulse falls down to a few mA before the transition to the spark. At higher frequencies, the maximum spark current decreases below  $1 \text{ A}$ , whereas the maximum streamer current does not change. The current decrease during the streamer-to-spark transition phase is also less significant. Sometimes, we even observed an almost instantaneous formation of a spark after the streamer with no current decrease in between. Finally, the resulting current pulse looks like two merging peaks (figure 6).

Because of the random character of the streamer-to-spark transition,  $\tau$  must be characterized by an average value, or even better by a probability distribution function  $\mathcal{P}(\tau)$ . Values of  $\tau$  shown in figure 5 actually correspond to a maximum of  $\mathcal{P}(\tau)$ . In order to obtain  $\mathcal{P}(\tau)$  we synchronized the acquisition of voltage and current waveforms by the rising edge of the streamer current measured on the  $50 \Omega$  resistor shunt. This moment was defined as the beginning of the streamer-to-spark transition event. The end of the transition was defined as the moment of maximum spark current.

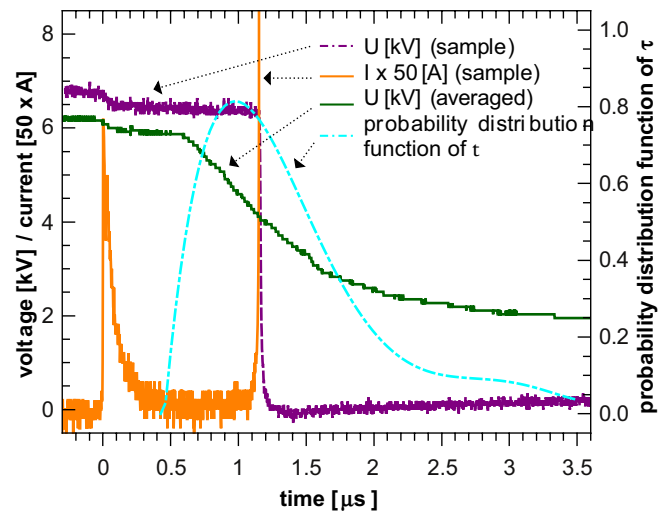


**Figure 7.** The estimate of probability distribution function of streamer-to-spark transition delay  $\tau$ , derived from the averaged voltage waveform (128 samples);  $f \approx 2.5 \text{ kHz}$ ,  $C = 32 \pm 4 \text{ pF}$ ,  $r = 1 \text{ k}\Omega$ ,  $d = 5.5 \text{ mm}$ ,  $R = 8.2 \text{ M}\Omega$ .

If we acquire an averaged current waveform from a few hundreds of TS pulses synchronized by the rising edge of the streamer, we get a well smoothed streamer pulse followed by a distribution function of spark current after the streamer. Based on our definition of  $\tau$ , this spark current distribution function corresponds in the first approximation to  $\mathcal{P}(\tau)$ .

We had to cut off the current during the spark phase to protect the oscilloscope, when we measured current on the  $50 \Omega$  shunt. Thus, we had to use voltage waveforms to calculate the spark current according to equation (2). In order to obtain a more accurate derivation of  $U$ , we first fitted the region with the voltage drop by a polynomial function. For example, figure 7 shows  $\mathcal{P}(\tau)$  at  $2.5 \text{ kHz}$  ( $d = 5.5 \text{ mm}$ ,  $R = 8.2 \text{ M}\Omega$ ). A difference between the single pulse and averaged waveforms is also demonstrated here.

In reality, the distribution functions of the current after the streamer are not identical with  $\mathcal{P}(\tau)$ . However, the difference between these two functions is certainly negligible below the

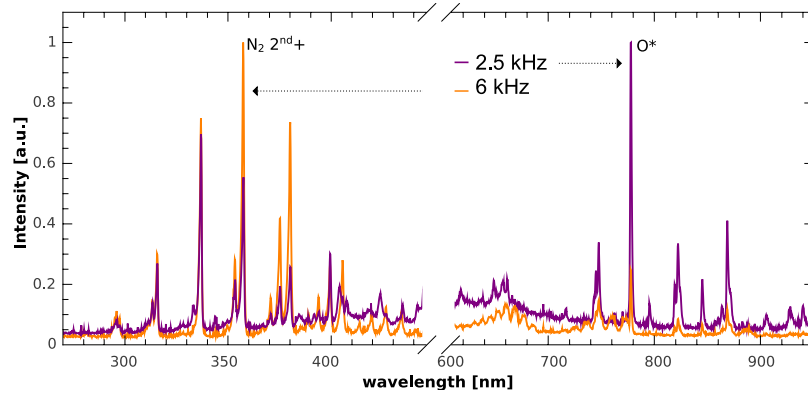


**Figure 8.** Time-integrated spectra of the TS discharge.

TS repetition frequency of around 4 kHz. In this region the duration of a single TS spark current pulse is very short compared with the typical streamer-to-spark transition time. At higher TS frequencies, a better approximation of  $\mathcal{P}(\tau)$  could be achieved by deconvolution of the measured spark current distribution function with the average spark current pulse measured on the  $1 \Omega$  resistor shunt with triggering on its own rising edge. We tested this approach using the broadest spark pulse and the narrowest spark current distribution function (at  $f \approx 8$  kHz), and we found that even here we can consider the spark current distribution function to be a good approximation of  $\mathcal{P}(\tau)$ .

Finally, it might be more appropriate to define  $\tau$  as the moment when the spark current starts to grow, not when it reaches the peak value. However, the resulting difference is again negligible at low TS frequencies, thanks to the steep spark current rise time (a few ns). This difference grows with increasing  $f$ , but we estimate that even at  $\sim 10$  kHz, it is only about 10% of  $\tau$  as it is defined. Thus, the value of  $\tau$  obtained using the second definition would be at most  $\sim 10$  ns lower compared with what we present here (figure 5).

### 3.4. Optical emission study of the TS

Significant differences between lower and higher frequency regimes of the TS were observed in time-integrated emission spectra in the VIS region (figure 8). The emission of O, N and  $N^+$  atomic lines dominated in the spectra at lower frequencies ( $< 3$  kHz). At higher frequencies these atomic lines almost disappeared, and the  $N_2$  first positive system ( $B^3\Pi_g - A^3\Sigma^+$ ) was much stronger. In the UV region, the  $N_2$  second positive system ( $C^3\Pi_u - B^3\Pi_g$ ) dominated at all frequencies, but its relative intensity compared with atomic lines in VIS region also increased significantly with  $f$ .

**3.4.1. PMT measurements of time evolution of emission intensity.** In order to explain the disappearance of atomic lines with increasing  $f$ , we used PMT with appropriate narrowband interference filters to measure the time evolution of the emission from  $O(^5P)$  species at 777 nm (the strongest atomic line), and from  $N_2(C)$  species ( $0-0$  band of the  $N_2$  second positive system at 337 nm). At lower frequencies (figure 9(a)), we can clearly see two peaks of total emission.

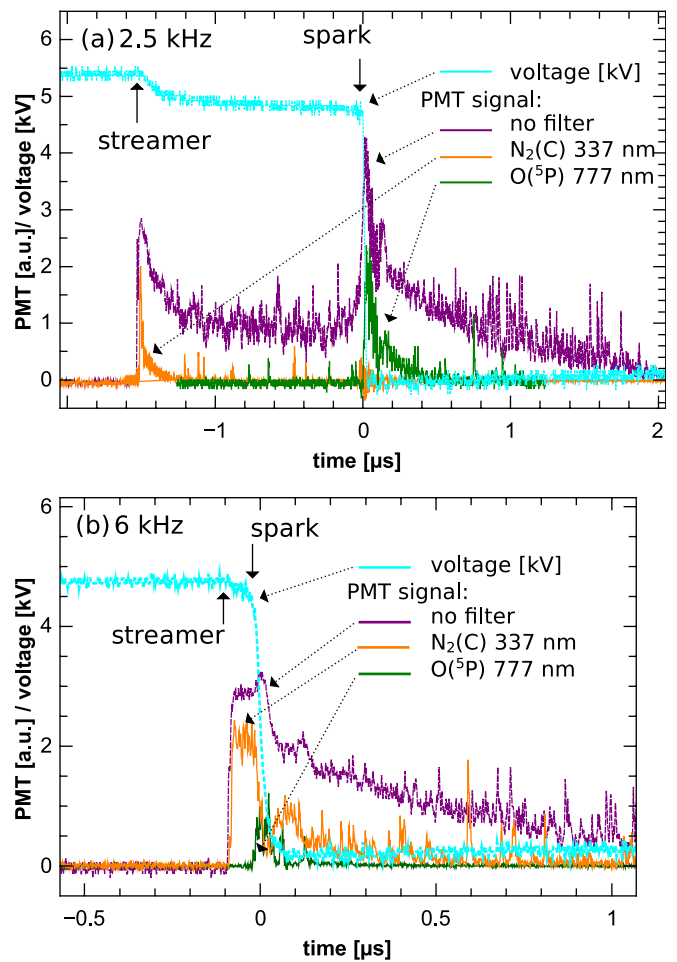


**Figure 9.** Typical PMT emission signals of the TS at (a) 2.5 kHz and (b) 6 kHz;  $R = 6.6 \text{ M}\Omega$ ,  $C = 26 \pm 4 \text{ pF}$ ,  $d = 5 \text{ mm}$ ,  $r = 0 \text{ k}\Omega$ .

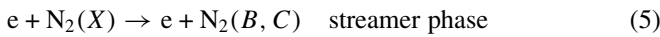
The first one is produced by the streamer, whereas the second one corresponds to the short spark. As  $f$  increases, these two emission peaks merge and cannot be easily distinguished at higher  $f$  (figure 9(b)). This can be explained by the shortening of the streamer-to-spark transition time  $\tau$  with growing  $f$ .

The time-integrated PMT signal from the  $O(^5P)$  species decreases with  $f$  quite significantly, whereas the signal from  $N_2(C)$  does not change much. This confirms the previous observation from time-integrated spectra (figure 8). New

information is that the  $N_2(C)$  species are produced mainly during the streamer phase and  $O(^5P)$  species during the spark phase (figure 9). The electrical properties of streamers, the rise time and the maximum current, do not change significantly with  $f$  (figure 6). In contrast, the spark current pulses are smaller and broader with  $f$ . For this reason we suppose that changes in the spark phase of the TS at higher  $f$  are responsible for the disappearance of the atomic lines in the time-integrated emission spectra.

Based on the work of Naidis [53], we suppose that the highest  $E/N$  is reached at the moment of the maximum of the spark current. Afterwards,  $E/N$  and the electron mean energy decline. The electron-impact excitation processes after the current peak value are therefore certainly less efficient than before. The broadening of the TS spark pulses with  $f$  is mostly due to the longer current decay time. This means that the overall efficiency (or capability) of the TS pulses to excite ground state atomic oxygen species decreases with increasing  $f$ . From this we can deduce an overall weaker chemical effect of the TS with smaller and broader pulses at higher  $f$ , which is in agreement with the observed decreasing decontamination efficiency [54].

Another possible explanation for the disappearance of oxygen atomic lines with increasing  $f$  might be a more complicated mechanism of  $O(^5P)$  generation. We suggest the following three-step mechanism, based on experimental study of  $O(^3P)$  generation by a nanosecond repetitively pulsed discharge [55]:



As the streamer-to-spark transition phase shortens with growing  $f$ , fewer  $O(^3P)$  atoms would accumulate for the production of  $O(^5P)$  during the high current phase.

**3.4.2. Changes in the gas temperature with  $f$ .** We used the emission spectra of the 0-0 band of the  $N_2$  second positive system at 337 nm, obtained by a spectrometer coupled with the iCCD camera, for the calculation of time-resolved rotational temperature  $T_r$  of the  $N_2(C)$  species. We obtained it by fitting the experimental spectra with the simulated ones using the Specair program [56]. We further assumed that in atmospheric-pressure air plasma  $T_r \approx T_g$ , where  $T_g$  is the gas temperature.

We can synchronize the iCCD camera with either the beginning of the streamer or the beginning of the spark phase. We were thus able to measure the initial temperatures (5–15 ns time window) at which streamers start ( $T_r^{\text{str}}$ ), as well as a temperature in the initial phase of the spark ( $T_r^{\text{spark}}$ ).  $T_r^{\text{spark}}$  represents approximately the breakdown temperature to the spark, while  $T_r^{\text{str}}$  represents approximately a ‘steady-state’ temperature to which gas is heated by the previous TS pulse. Figure 10 shows dependences of these temperatures on  $f$ .

The initial streamer temperature  $T_r^{\text{str}}$  obviously increased with  $f$ , though the overall heating of the gas was not very significant. Even at 10 kHz, the ‘steady-state’ temperature at which every new streamer initiating the TS starts is only

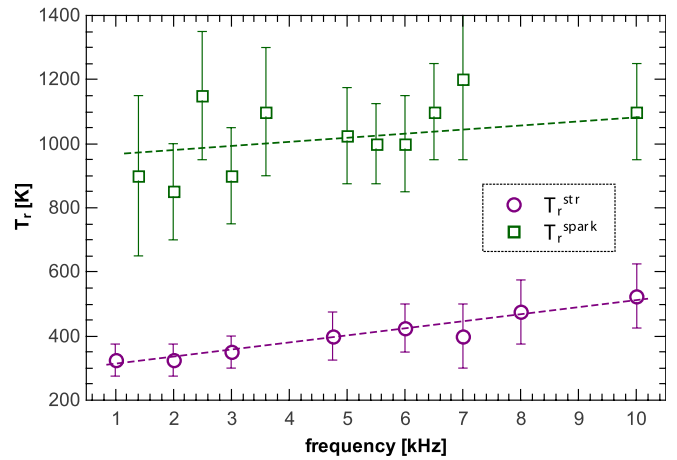


**Figure 10.** Changes of the rotational temperature of  $N_2(C)$  species with  $f$ :  $T_r^{\text{str}}$ , measured during the initial 5–20 ns of the streamer,  $T_r^{\text{spark}}$ , measured during the initial 20 ns of the spark;  $R = 8.2 \text{ M}\Omega$ ,  $C = 32 \pm 4 \text{ pF}$ ,  $d = 5 \text{ mm}$ ,  $r = 1 \text{ k}\Omega$ .

around 550 K. However, this slight increase in temperature can explain the decrease in  $U_{\text{TS}}$  with growing  $f$ . At higher temperatures, lower  $U_{\text{TS}}$  is required to keep  $E/N$  constant, thanks to the decrease in  $N$  resulting from the increase in the gas temperature.

The decrease in  $N$  can also explain the broadening of current pulses with increasing  $f$  (figure 4). The rate of chemical processes, including ionization or recombination, typically depends on the product of densities of the reactants. Lower densities would therefore lead to a longer build-up of the charge as well as to its longer decay. The area of the current pulse is proportional to the product of  $C$  and  $U_{\text{TS}}$ . Even if  $U_{\text{TS}}$  was constant, broader current peaks must be smaller. The decrease in  $U_{\text{TS}}$  only enhances the decrease in  $I_{\text{max}}$  with increasing  $f$  (figure 3).

Although it seems that  $T_r^{\text{spark}}$  also slightly increases with  $f$ , the uncertainty in these data is quite high. Within the experimental error, we can conclude that the breakdown temperature at the beginning of the spark is constant:  $T_r^{\text{spark}} = 1000 \pm 125 \text{ K}$ . We thus suppose that the increase in  $T_g$  to  $\sim 1000 \text{ K}$  is crucial for the streamer-to-spark transition. There are two possible reasons for this: an increase in  $E/N$  in the plasma column generated by the streamer due to the decrease in  $N$ , or changes in the gas phase chemistry.

Under the assumption of constant atmospheric pressure, we estimated that an averaged  $E/N$  in the plasma channel would increase from about 60 Td to about 170 Td, while going from streamer to spark due to the increase in  $T_g$  from around 350 to 1000 K. In reality, we should also take into account changes of the pressure inside the plasma channel. A pulsed discharge similar to a TS was recently simulated by Naidis [53]. During the spark phase, at the moment of the highest  $E/N$ , the pressure on the axis of the plasma channel was almost 2 bars. If we used this value, we would get an increase in average  $E/N$  to only about 100 Td instead of 170 Td. The spark breakdown could therefore also be related to the changes in chemistry at higher  $T_g$ . The observed breakdown temperature corresponds very well with the critical

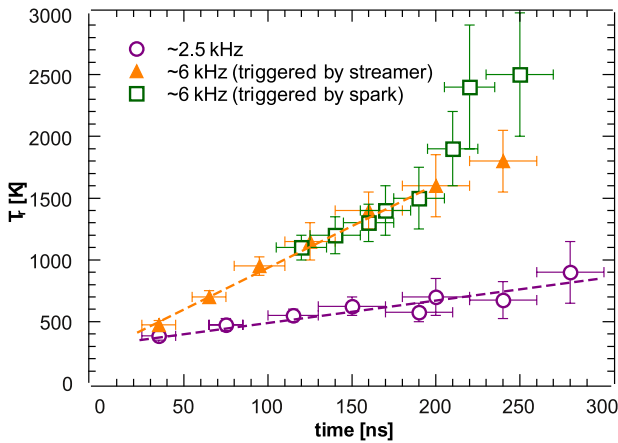


**Figure 11.** Changes of rotational temperature of the  $N_2(C)$  species with time;  $R = 8.2 \text{ M}\Omega$ ,  $C = 32 \pm 4 \text{ pF}$ ,  $d = 5 \text{ mm}$ ,  $r = 1 \text{ k}\Omega$ .

temperature necessary to overcome the electron affinity by thermal detachment reactions. Probably both the increase in  $E/N$  and the acceleration of thermal electron detachment play a certain role. Further research on the TS, including kinetic modeling, is necessary to resolve this question.

**3.4.3. Changes in temperature after the streamer.** From  $T_r^{\text{spark}}$  and  $T_r^{\text{str}}$  it is obvious that the temperature increases after the streamer. We therefore measured the time evolution of  $T_r$  during the transition time for various fixed discharge frequencies (figure 11). A decreasing intensity of  $N_2(C)$  emission enabled us to follow  $T_r$  only for about 300 ns from the beginning of the streamer. At higher frequencies, where the transition time  $\tau < 200 \text{ ns}$ , we also measured the time evolution of  $T_r$  with the camera triggered by the beginning of the spark pulse, although we still observed light from the  $N_2(C)$  species generated by the streamer. At lower frequencies, where  $\tau > 300 \text{ ns}$ , it was not possible to follow the evolution of  $T_r$  during the whole streamer-to-spark transition phase. Here we were therefore able to measure  $T_r^{\text{spark}}$  only thanks to the small amount of  $N_2(C)$  species produced during the initial phase of spark.

At both  $f = 2.5 \text{ kHz}$  and  $6 \text{ kHz}$  (figure 11), we observed approximately a linear increase in  $T_r$  with time before the breakdown. The heating is faster at  $6 \text{ kHz}$ , although in both cases the streamer-to-spark transition occurs when  $T_r \approx 1000 \text{ K}$ . The acceleration of gas heating with growing  $f$  is probably the major reason for the shortening of  $\tau$  with  $f$ , though it can be partially attributed to the increase in  $T_r^{\text{str}}$ .

We suppose that the gas heating is caused by the electric current flowing through the generated plasma channel (Joule heating). The acceleration of gas heating with growing  $f$  can therefore be explained by the increase in average current during the streamer-to-spark transition phase: figure 6 illustrates this phenomenon. At  $3 \text{ kHz}$ , the current after the streamer peak value decreases quickly to around  $10 \text{ mA}$  and it stays at this value during the remaining streamer-to-spark transition phase. At  $5 \text{ kHz}$ , the current decrease after the streamer was much slower. The current only decreased to  $\sim 130 \text{ mA}$  before it started to slowly climb again. At higher frequencies, the current sometimes does not decrease at all and starts to grow slowly right after the streamer.

The reaction rate is given by the product of the rate coefficients with the concentrations of the reactants. The slower current decay after streamers at higher TS frequencies can be therefore explained by the decrease in the gas density  $N$  due to the increase in  $T_r^{\text{str}}$ , even if the rate coefficients were not influenced. Because of the temperature dependence of their rate coefficients, the recombination reactions could be even more suppressed by the increase in the gas temperature to  $\sim 500 \text{ K}$ . However, this cannot explain why we sometimes observed no current decay at all above  $5 \text{ kHz}$ . It means that processes generating electrons must be accelerated with increasing  $f$ .

We estimated the average  $E/N$  to be around  $60\text{--}70 \text{ Td}$  in the plasma channel right after its establishment by a streamer, assuming a uniform axial distribution of the reduced electric field. This is certainly not enough for direct electron-impact ionization processes to play an important role. The most probable explanation for the instantaneous current increase is therefore a chemical or stepwise ionization thanks to species accumulated from previous TS pulses, i.e. a memory effect.

We admit that the assumption of the uniform axial distribution of  $E/N$  is very rough. There is certainly a stronger field around the needle electrode, and this should propagate towards the grounded electrode as a secondary streamer. However, the development of the secondary streamer takes several tens of ns [12], and we observed an almost instantaneous increase in the current. The secondary streamer could be the main breakdown mechanism only if its propagation is significantly accelerated at higher  $f$ . However, this could also be caused by the memory effect. Further research is required to answer this question.

## 4. Conclusions

We investigated the electrical characteristics and time-resolved optical emission of a dc-supplied periodic streamer-to-spark transition discharge in atmospheric air, called a transient spark (TS). Thanks to the small internal capacity of the discharge gap and a limiting series resistor, the TS is characterized by a very short spark pulse duration ( $\sim 10\text{--}100 \text{ ns}$ ) with peak current  $1\text{--}10 \text{ A}$ . The TS can be maintained under low energy conditions ( $0.1\text{--}1 \text{ mJ pulse}^{-1}$ ) and the generated plasma cannot therefore reach LTE conditions, despite the fact that the current pulse can lead to a temporary increase in gas temperature up to  $\sim 2500 \text{ K}$ . The steady-state temperature, however, remains relatively low, since even at high repetition frequencies ( $\sim 10 \text{ kHz}$ ) each streamer-to-spark process starts at  $\sim 550 \text{ K}$ . A subsequent increase in temperature to  $\sim 1000 \text{ K}$  governs the streamer-to-spark transition. This can be explained either by the increase in  $E/N$  due to decreasing  $N$ , or by thermal electron-detachment reactions.

The shortening of the average streamer-to-spark transition time with increasing TS frequency can be partly explained by the slight increase in  $T_r^{\text{str}}$ , and mostly by an acceleration of the temperature growth. The acceleration of heating is caused by the changes of current waveforms during the streamer-to-spark phase. At  $3 \text{ kHz}$ , the current after the streamer peak decays quite quickly to around  $10 \text{ mA}$ , whereas at  $6 \text{ kHz}$ , it

sometimes does not decay at all and starts to grow right after the streamer. Just a few tens of nanoseconds later, this increase accelerates and the breakdown occurs. There appears almost a continuous transition from streamer to spark. We suppose that this behavior can be partly explained by the decrease in the gas density due to the increase in the gas temperature. It is also necessary to consider changes in the gas phase chemistry due to the increase in the gas temperature, and a memory effect: an accumulation of some species (NO, O<sub>2</sub>(a), etc) that favor the ionization processes and thus shorten the transition phase. Further research is required, including new analytic techniques and a kinetic modeling, to explain the role of the increasing initial gas temperature and of the increasing TS frequency on the breakdown mechanism.

## Acknowledgments

This work is sponsored by the Slovak Research and Development Agency APVV SK-FR-0038-09, and Slovak grant agency VEGA 1/0668/11 and 1/0998/12. Our special thanks go to Dr Emmanuel Marode for fruitful discussions and his advice.

## References

- [1] Penetrante B and Schultheis S E 1993 (eds) *Non-Thermal Plasma Techniques for Pollution Control (NATO ASI Series G34 vol 1)* (New York: Springer)
- [2] Lowke J J and Morrow R 1995 *IEEE Trans. Plasma Sci.* **23** 661–71
- [3] Kogelschatz U 2003 *Plasma Chem. Plasma Process.* **23** 1
- [4] Meek J M 1940 *Phys. Rev.* **57** 722–8
- [5] Morrow R and Lowke J J 1997 *J. Phys. D: Appl. Phys.* **30** 614–27
- [6] Kulikovskiy A A 1998 *IEEE Trans. Plasma Sci.* **26** 1339–46
- [7] Peek F W Jr 1929 *Phenomena in High Voltage Engineering* (New York: McGraw-Hill)
- [8] Llewellyn-Jones F 1966 *Ionization and Breakdown in Gases* (London: Methuen)
- [9] Meek J M and Craggs J D 1978 *Electrical Breakdown of Gases* (New York: Wiley)
- [10] Raether H 1964 *Electron Avalanches and Breakdown in Gases* (London: Butterworths)
- [11] Loeb L B 1965 *Electrical Coronas* (Berkeley, CA: University of California Press)
- [12] Marode E 1975 *J. Appl. Phys.* **46** 2005  
Marode E 1975 *J. Appl. Phys.* **46** 2016
- [13] Lowke J J 1992 *J. Phys. D: Appl. Phys.* **25** 202
- [14] Larsson A 1998 *J. Phys. D: Appl. Phys.* **31** 1100–8
- [15] Naidis G V 1999 *J. Phys. D: Appl. Phys.* **32** 2649–54
- [16] Aleksandrov N L and Bazelyan E M 1999 *Plasma Sources Sci. Technol.* **8** 285–94
- [17] Kulikovskiy A A 2001 *IEEE Trans. Plasma Sci.* **29** 313–17
- [18] Bourdon A, Bonaventura Z and Celestine S 2010 *Plasma Sources Sci. Technol.* **19** 034012
- [19] Efremov N M, Adamiak B Y, Blochin V I, Dadashev S J, Dmitriev K I, Gryaznova O P and Jusbashev V F 2000 *IEEE Trans. Plasma Sci.* **28** 238
- [20] Wagner H-E, Brandenburg R, Kozlov K V, Sonnenfeld A, Michel P and Behnke J F 2003 *Vacuum* **71** 417
- [21] Mizuno A, Clements J S and Davis R H 1986 *IEEE Trans. Industry Appl.* **22** 516–22
- [22] Penetrante B M, Bardsley J N and Hsiao M C 1997 *Japan J. Appl. Phys.* **36** 5007–17
- [23] Masuda S and Nakao H 1990 *IEEE Trans. Industry. Appl.* **26** 374–83
- [24] Walsh J L, Shi J J and Kong M G 2006 *Appl. Phys. Lett.* **89** 161505
- [25] Pancheshnyi S V, Lacoste D A, Bourdon A and Laux C O 2006 *IEEE Trans. Plasma Sci.* **34** 2478–87
- [26] Pai D, Lacoste D A and Laux C O 2008 *IEEE Trans. Plasma Sci.* **36** 974–5
- [27] Bastien F and Marode E 1979 *J. Phys. D: Appl. Phys.* **12** 249
- [28] Machala Z, Morvová M, Marode E and Morva I 2000 *J. Phys. D: Appl. Phys.* **33** 3198
- [29] Machala Z, Marode E, Laux C O and Kruger C H 2004 *J. Adv. Oxid. Technol.* **7** 133
- [30] Yu L, Laux C O, Packan D M and Kruger C H 2002 *J. Appl. Phys.* **91** 2678
- [31] Staack D, Farouk B, Gutsol A and Fridman A 2005 *Plasma Sources Sci. Technol.* **14** 700
- [32] Akishev Yu, Grushin M, Karalnik V, Petryakov A and Trushkin N 2010 *J. Phys. D: Appl. Phys.* **43** 075202
- [33] Marode E, Goldman A and Goldman M 1993 High pressure discharge as a trigger for pollution control *Non-Thermal Plasma Techniques for Pollution Control (NATO ASI series Part A)* ed B Penetrante and S E Schultheis (Berlin: Springer)
- [34] Hafez R, Samson S and Marode E 1995 A prevented spark reactor for pollutant control. Investigation of NO<sub>x</sub> removal *Proc. 12th ISPC (Minneapolis, MN)*, vol 2, pp 855–61
- [35] Marode E 2012 The prevented spark plasma in atmospheric air: from field to thermal equilibrium *Plasma for Environmental Issues* ed E Tatarova et al (Sofia: Artgraf)
- [36] Pai D, Stancu G D, Lacoste D A and Laux C O 2009 *Plasma Sources Sci. Technol.* **18** 045030
- [37] Janda M and Machala Z 2008 *IEEE Trans. Plasma Sci.* **36** 916
- [38] Janda M, Martišovič V and Machala Z 2011 *Plasma Sources Sci. Technol.* **20** 035015
- [39] Laux C O, Spence T G, Kruger C H and Zare R N 2003 *Plasma Sources Sci. Technol.* **12** 125
- [40] Fantz U 2006 *Plasma Sources Sci. Technol.* **15** S137
- [41] Marode E, Samson S, Djermoune D, Deschamps N and Touzeau M 1999 *J. Adv. Oxid. Technol.* **4** 305–11
- [42] Mitchell J B A 1990 *Phys. Rep.* **186** 215
- [43] Johnsen R 1993 *J. Chem. Phys.* **98** 5390
- [44] Sigmond S R 1984 *J. Appl. Phys.* **56** 1355
- [45] Bastien F and Marode E 1985 *J. Phys. D: Appl. Phys.* **18** 377
- [46] Marode E, Djermoune D, Dessante P, Deniset C, Segur P, Bastien F, Bourdon A A and Laux C 2009 *Plasma Phys. Control. Fusion* **51** 124002
- [47] Ono R and Oda T 2007 *J. Phys. D: Appl. Phys.* **40** 176
- [48] Marode E, Bastien F and Bakker M 1979 *J. Appl. Phys.* **50** 141–6
- [49] Gallimberti I 1979 *J. Physique* **40** 193
- [50] Raizer Yu P 1991 *Gas Discharge Physics* (Berlin: Springer)
- [51] Bondiou A and Gallimberti I 1994 *J. Phys. D: Appl. Phys.* **27** 1252
- [52] Goelian N, Lalande P, Bondiou-Clergerie A, Bacchiega G L, Gazzani A and Gallimberti I 1997 *J. Phys. D: Appl. Phys.* **30** 2441
- [53] Naidis G V 2009 *Eur. Phys. J. Appl. Phys.* **47** 22803
- [54] Machala Z, Jedlovský I, Chládeková L, Pongráč B, Giertl D, Janda M, Šikurová L and Polčič P 2009 *Eur. Phys. J. D* **54** 195
- [55] Stancu G D, Kaddouri F, Lacoste D A and Laux C O 2010 *J. Phys. D: Appl. Phys.* **43** 124002
- [56] Laux C O 2002 Radiation and nonequilibrium collisional-radiative models *Physico-Chemical Modeling of High Enthalpy and Plasma Flows* (Lecture Series 2002–07) (Rhode-Saint-Gense, Belgium: von Karman Institute)